Gyrokinetic TEM stability calculations for quasi-isodynamic stellarators

J H E Proll[1], P Helander[1], P Xanthopoulos[1] and J W Connor[2,3]

[1] Max-Planck-Institut für Plasmaphysik, EURATOM Association, Teilinstitut Greifswald, Wendelsteinstraße 1, 17491 Greifswald, Germany
[2] Culham Centre for Fusion Energy, Abingdon OX14 3DB, United Kingdom
[3] Imperial College of Science, Technology and Medicine, London SW7 2BZ, United Kingdom

E-mail: josefine.proll@ipp.mpg.de

Abstract. Recent theoretical findings suggest that in perfectly quasi-isodynamic stellarators, the trapped-particle instability as well as the ordinary electron-density-gradient-driven trapped-electron mode are stable in the electrostatic and collisionless approximation. In these configurations contours of constant magnetic field strength B are poloidally closed, the second adiabatic invariant J is constant on flux surfaces and peaks in the centre. It follows that the diamagnetic drift frequency ω_{*a} and the bounce-averaged magnetic drift frequency $\overline{\omega_{da}}$ are in opposite directions, $\omega_{*a} \cdot \overline{\omega_{da}} < 0$, everywhere on the flux surface. This is the signature of average "good curvature" for trapped particles and, thanks to this property, particles that bounce faster than the frequency of any unstable mode must draw energy from it near marginal stability. Consequently, the point of marginal stability cannot exist for the collisionless trapped-particle mode, and hence this mode will be absent. By a similar argument, the ordinary trapped-electron mode is also stable. Because perfect quasi-isodynamicity can never be reached, it is necessary to test configurations approaching quasi-isodynamicity numerically in order to probe their resilience against trapped-particle modes. Progress has been made to extend gyrokinetic simulations to stellarator geometries, enabling us to perform the first linear gyrokinetic simulations of density-gradient-driven modes in stellarator configurations approaching quasi-isodynamicity, such as Wendelstein 7-X and more recently found configurations. These simulations appear to confirm the analytical predictions.

1. Introduction

Plasma confinement in a stellarator is achieved through a three-dimensionionally shaped magnetic field, rather than an axisymmetric field as in a tokamak. Due to this property stellarators usually suffer from higher levels of collisional (so-called neoclassical) transport than tokamaks. However, in recent numerically optimised stellarator configurations [1], the neoclassical transport is on par with axisymmetric devices (unless the collisionality is very low). An important class of these optimised stellarators are the quasi-isodynamic ones. It was shown recently [2] that in these stellarator configurations, the collisionless trapped-particle instability as well as the ordinary electron-density-gradient-driven trapped-electron mode (TEM) are stable, provided the temperature gradients are small enough compared with the density gradient. Since these instabilities - in combination with ion and electron-temperature gradient (ITG and ETG) modes - are believed to be the cause for much of the turbulence in tokamaks, quasi-isodynamic stellarators could also enjoy reduced turbulent transport.

A quasi-isodynamic field is characterised by poloidally, but not toroidally, closed contours of maximum and minimum magnetic field strength $B = |\mathbf{B}|$ and confinement of all collisionless orbits

[3, 4]. The second adiabatic invariant,

$$J = \int_{l_1}^{l_2} m v_\parallel dl,$$

where the integral is taken between two bounce points, is then constant on flux surfaces. If the magnetic field is given by $\mathbf{B} = \nabla\psi \times \nabla\alpha$, where ψ is the toroidal flux and α denotes the field line label, we can define the magnetic drift frequency $\omega_{da} = \mathbf{k}_\perp \cdot \mathbf{v}_{da}$ and the drift wave frequency $\omega_{*a} = (T_a k_\alpha / e_a) d\ln n_a / d\psi$ for each particle species a in the usual way, where the density n_a and temperature T_a are constant on flux-surfaces, and $\mathbf{v}_{da} = \hat{\mathbf{b}} \times ((v_\perp^2/2)\nabla \ln B + v_\parallel^2 \boldsymbol{\kappa})/\Omega_a$ denotes the drift velocity, with $\hat{\mathbf{b}} = \mathbf{B}/|\mathbf{B}|$ the unit tangent vector and $\boldsymbol{\kappa} = \hat{\mathbf{b}} \cdot \nabla\hat{\mathbf{b}}$ the curvature vector of the magnetic field. The wave vector perpendicular to the magnetic field is given by $\mathbf{k}_\perp = k_\alpha \nabla\alpha + k_\psi \nabla\psi$. In quasi-isodynamic configurations, the precessional drift frequency of the particles $\overline{\omega_{da}}$, where an overbar denotes the bounce average, is usually in the opposite direction to the diamagnetic drift frequency ω_{*a} everywhere on the flux surface. Trapped particles therefore experience an average "good curvature" and, if their bounce frequency ω_{ba} exceeds the frequency of any unstable mode, must draw energy from it near marginal stability. It is thus concluded that quasi-isodynamic stellarators are resilient against the ordinary TEM and collisionless trapped-particle mode [2]. Here we embark on the numerical validation of this finding by performing linear gyrokinetic simulations of these modes in stellarator geometries. This is important since perfect quasi-isodynamicity can never be realised and it is interesting to investigate how well these analytical findings apply to actual configurations such as those conceived in the last few years [1, 4, 5] and also in Wendelstein 7-X. In Section 2, we present a condensed version of the analytical calculation that lead to the result above. In Section 3, the simulation setup is explained, the results and mode analysis are presented in Section 4, and are summarised in the final Section 5.

2. Analytical considerations

We now briefly revisit the calculation why the non-resonance of the two characteristic frequencies of the system

$$\omega_{*a} \cdot \overline{\omega_{da}} < 0. \tag{1}$$

leads to resilience against trapped-particle modes. For the detailed calculation the reader is referred to [2]. The calculation is based upon the gyrokinetic equation in ballooning space,

$$i v_\parallel \nabla_\parallel g_a + (\omega - \omega_{da}) g_a = \frac{e_a \phi}{T_a} J_0(k_\perp v_\perp / \Omega_a) \left(\omega - \omega_{*a}^T\right) f_{a0}, \tag{2}$$

together with the quasi-neutrality condition,

$$\sum_a \frac{n_a e_a^2}{T_a} \phi = \sum_a e_a \int g_a J_0 \mathrm{d}^3 v. \tag{3}$$

Here ϕ is the electrostatic potential, J_0 is the zeroth order Bessel function of the first kind, $g_a = f_{a1} + \frac{e_a\phi}{T_a} f_{a0}$ denotes the non-adiabatic part of the perturbed distribution function, and the equilibrium distribution function f_{a0} is Maxwellian. The ratio between the temperature and density gradients is denoted by $\eta_a = d\ln T_a / d\ln n_a$, and we have written $\omega_{*a}^T = \omega_{*a}[1 + \eta_a(x^2 - 3/2)]$, with $x^2 = m_a v^2 / 2T_a$. From the gyrokinetic equation we can obtain a quantity

$$P_a = e_a \mathrm{Im}\left\{(i v_\parallel \nabla_\parallel g_a - \omega_{da} g_a)\phi^* J_0\right\}, \tag{4}$$

which, following [6], can be understood as the gyrokinetic energy transfer from the electrostatic fluctuations to species a. Here we use the notation

$$\{\cdots\} = \int_{-\infty}^{\infty} \frac{\mathrm{d}l}{B} \int (\cdots) d^3 v.$$

When P_a is directly obtained from the gyrokinetic equation and we sum over all species, we find for a complex mode frequency $\omega = \omega_r + i\gamma$ a relation for the energy budget of the fluctuations,

$$-\gamma \sum_a \frac{n_a e_a^2}{T_a} \int \frac{\mathrm{d}l}{B} (1 - \Gamma_0) |\phi|^2 = \sum_a P_a, \tag{5}$$

where $b = k_\perp^2 T_a / m_a \Omega_a^2$ and

$$\Gamma_0(b) = n_a^{-1} \int J_0^2 f_{a0} d^3v < 1.$$

For a positive growth rate we thus require the sum on the right-hand side to be negative. For particles that bounce faster than the frequency of the mode, $\omega \ll \omega_{ba}$, which allows the ordering $\omega \sim \omega_{*a} \ll k_\parallel (T_a/m_a)^{1/2}$, we can find a solution for the distribution function g_a where we can neglect the passing particle contribution. We therefore obtain

$$P_a = \frac{e_a^2}{T_a} \mathrm{Im} \left\{ (\omega - \omega_{*a}^T) \left(\overline{|J_0 \phi|^2} - \frac{\omega |\overline{J_0 \phi}|^2}{\omega - \overline{\omega}_{da}} \right) f_{a0} \right\}. \tag{6}$$

If we now approach the point of marginal stability, $\gamma \to 0+$, we find

$$P_a = \frac{\pi e_a^2}{T_a} \left\{ \delta(\omega - \overline{\omega}_{da}) \overline{\omega}_{da} (\overline{\omega}_{da} - \omega_{*a}^T) |\overline{J_0 \phi}|^2 f_{a0} \right\}. \tag{7}$$

Let us now limit ourselves to scenarios where the temperature gradient is smaller than the density gradient, more specifically $0 < \eta_a < 2/3$, which ensures that ω_{*a} and ω_{*a}^T have the same sign for all energies. For quasi-isodynamic configurations, we know in addition that ω_{*a}^T and $\overline{\omega}_{da}$ are of opposite signs, consequently $P_a > 0$ and energy is transferred from the electrostatic fluctuations to the particles of plasma species a. For modes whose frequency is well below the bounce frequency of all plasma constituents $\omega \ll \omega_{ba}$ for all a - as for the collisionless trapped-particle mode - we therefore obtain $\sum_a P_a > 0$. However, according to Eq. (5) we expect $\sum_a P_a = 0$ at the point of marginal stability. Consequently, this point cannot exist, and neither can the corresponding mode. The special case where the real part of the mode frequency vanishes, $\omega_r = 0$, needs to be treated separately, but this mode can be ruled out as well. We have therefore shown the resilience of quasi-isodynamic configurations against the collisionless trapped-particle mode. In addition, by explicitly solving the gyrokinetic equation in general geometry, we can demonstrate that if there are any modes whose frequency is below the electron bounce frequency but comparable to or larger than the ion bounce frequency, $\omega_{bi} \simeq \omega \ll \omega_{be}$, in a quasi-isodynamic configuration, it must propagate in the ion diamagnetic direction and draw its energy from the ions rather than the electrons at marginal stability. The ordinary TEM is thus expected to be stable as well. Since it is known that perfect quasi-isodynamicity cannot be achieved, simulating trapped-particle modes in realistic configurations is essential. Even if most, but not all, orbits satisfy $\omega_{*e} \cdot \overline{\omega_{de}} < 0$ one would expect a reduced growth rate compared with a tokamak or a non-optimised stellarator.

3. The simulation setup

The simulations are performed with the gyrokinetic code GENE [7, 8]. For computational efficiency, field-aligned coordinates are used. Here, x corresponds to the flux label, z the coordinate along the field line and y the binormal coordinate. Since we are interested in collisionless, electrostatic instabilities, we neglect both collisions and magnetic fluctuations. (It was shown in tokamaks that the effect of the plasma β on TEMs is very small [9, 10].) We will, however, keep the full magnetic drift when using a high-β equilibrium, since our modes are expected to be highly sensitive to the sign of ω_{da}. Both the electrons and the ions are treated kinetically, and the mass ratio is $m_e/m_i = 5.4466 \cdot 10^{-4}$, which corresponds to a hydrogen plasma. The simulations are performed in a flux tube, therefore only a small fraction of

the surface is covered. While definite statements about the stability of the entire plasma cannot be made without the knowledge of the stability properties of the entire flux surface, flux tube simulations can give an estimate of the stability of a given magnetic geometry.

We investigate the stability of the six-periodic stellarator of Subbotin *et al.* - in a configuration very similar to that presented in [1] and with major and minor radii of $R_0 = 11.85\mathrm{m}$ and $a = 0.95\mathrm{m}$ respectively - and compare the performance of the vacuum case with a high - β case with $\beta = 6\%$. As we shall see, the configuration with $\beta = 6\%$ is nearly quasi-isodynamic whilst the vacuum field is not. In order to investigate the influence on microinstabilities, we will compare these in the $\alpha = 0$ flux tube on the surface at half radius of each configuration. In Fig. 1 and 2 the bounce averaged drift frequency $\overline{\omega_{de}}$ is shown for both cases, with the closed black lines denoting the zero contour and the open black line the magnetic field line with $\alpha = 0$.

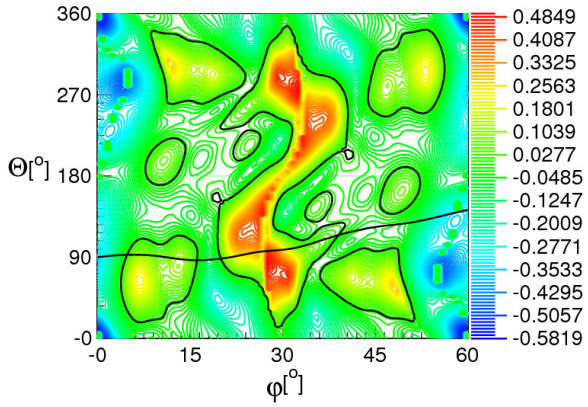

Figure 1. $\overline{\omega_{de}}$ for the vacuum configuration, shown as a function of the poloidal and toroidal angles at the bounce points

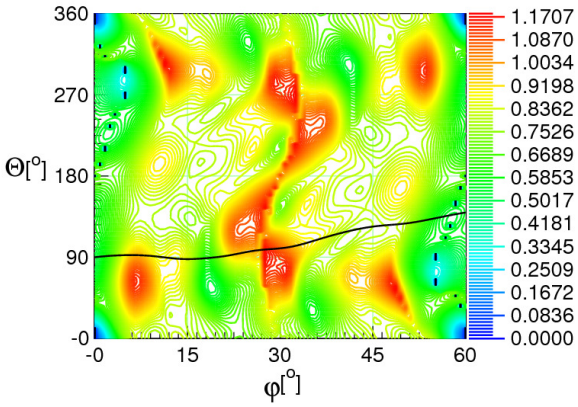

Figure 2. $\overline{\omega_{de}}$ for the high β configuration, shown as a function of the poloidal and toroidal angles at the bounce points

Note that in Fig. 2 there is no zero contour, and since ω_{*e} has been defined to be negative for conventional density gradients our stability criterion $\omega_{*a} \cdot \overline{\omega_{da}} < 0$ holds everywhere on the flux surface. It must be noted, however, that even though the $\beta = 6\%$ case comes very close to quasi-isodynamicity, the surfaces of constant J do not quite coincide with flux surfaces.

For both cases the shear $\hat{s}$ is very small, and in order to decrease the computational cost the simulations were limited to only one poloidal revolution. The modes were observed to decay sufficiently fast towards the edges of the flux tube, and did not change if the computational domain was extended to cover several turns around the torus.

4. Simulation results

4.1. Comparison of stability properties

For the simulations the normalised density gradient $a/L_n = -a\,\mathrm{d}\ln n/\mathrm{d}r$ with the minor radius a was varied simultaneously for both species between values of 0.0 and 3.0 In addition the normalised electron temperature gradient $a/L_{T_e} = -a\,\mathrm{d}\ln T_e/\mathrm{d}r$ was also varied between 0.0 and 3.0. The ion temperature profile was deliberately kept flat $a/L_{T_i} = 0$ to avoid the onset of ion-temperature-gradient-driven modes. For each pair of gradients we scanned over the binormal wave vector $k_y\rho = [0.1 \ldots 0.9]$ to find the most unstable mode (excluding the ETG mode, which has higher k_y). For comparison we also calculated the equivalent stability diagram for the Cyclone base case tokamak [11]. The stability diagram of this tokamak is displayed in Fig. 3. It can be seen that increasing the temperature gradient has a destabilising influence and that the highest growth rates slightly exceed $\gamma = 0.7c_s/a$, where c_s is the sound speed.

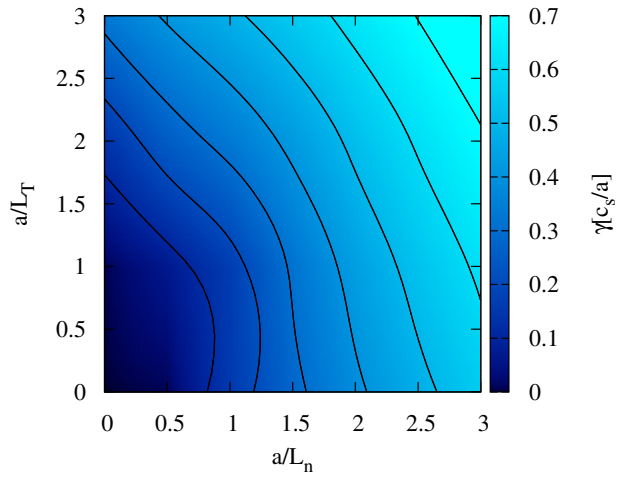

Figure 3. Stability diagram showing the growth rates of each most unstable low-frequency mode for the Cyclone base case tokamak. The lines denote the contours of $\gamma = 0.1c_s/a, \ldots, 0.7c_s/a$.

From the stability diagrams of the six-periodic stellarator, we see that the highest growth rates of the vacuum case (Fig. 4) are comparable to those in the tokamak. However, the electron temperature gradient is stabilising for the stellarator. In contrast, the high-β-case (Fig. 5) is hardly unstable at all. The fastest growing mode is found at $a/L_n = 3.0$ with a flat temperature profile and reaches a growth rate of mere $\gamma = 0.12\ c_s/a$.

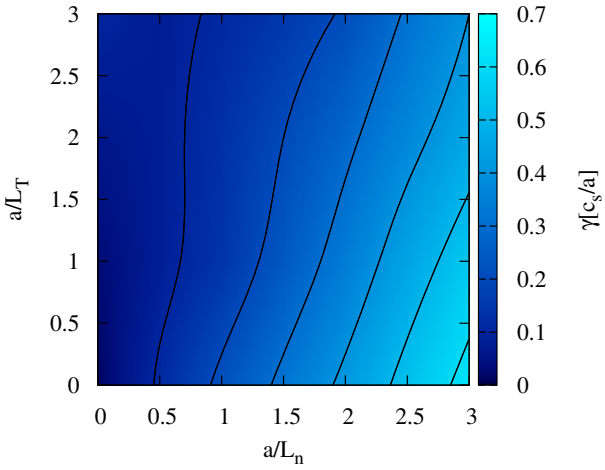

Figure 4. Stability diagram showing the growth rates of each most unstable mode for the vacuum configuration. The lines denote contours of $\gamma = 0.1c_s/a, \ldots, 0.6c_s/a$.

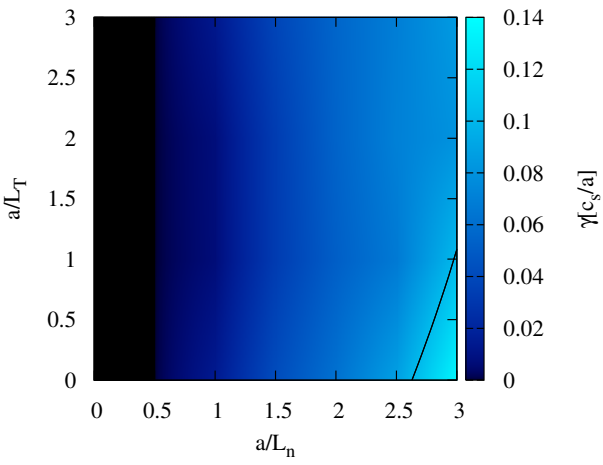

Figure 5. Stability diagram showing the growth rates of each most unstable mode for the high β configuration. The line denotes the $\gamma = 0.1c_s/a$ - contour.

The improved stability of the high-β-case becomes even more evident when one juxtaposes the density gradient scans at different temperature gradients for the two configurations. To display the influence of the density gradient more clearly, only one $k_y\rho$ is chosen for each temperature gradient.

From Fig. 6 we conclude that the temperature gradient acts stabilising unless the density gradient is very small. We also see that there is no critical density gradient for the vacuum configuration. The high-β-case on the other hand clearly has a critical density gradient at $a/L_n = 0.5$, but even above this

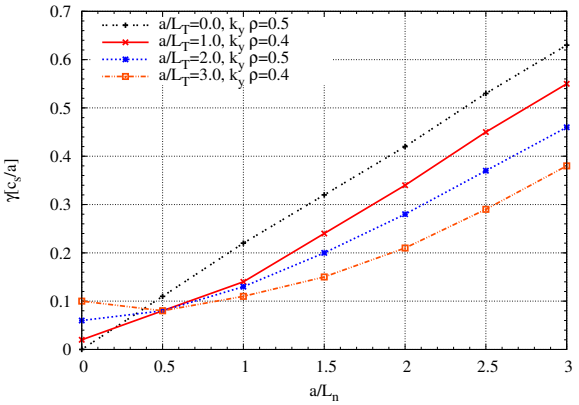

Figure 6. Density gradient scans for different temperature gradients for the vacuum configuration

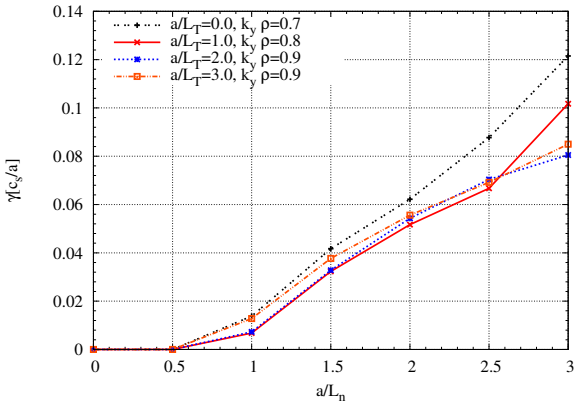

Figure 7. Density gradient scans for different temperature gradients for the high β configuration

gradient do the growth rates remain far below the vacuum case.

4.2. Mode analysis

The structure of the electrostatic potential of most of the modes observed (Fig. 8), where the peaks coincide with magnetic wells, clearly hints at a trapped-particle mode.

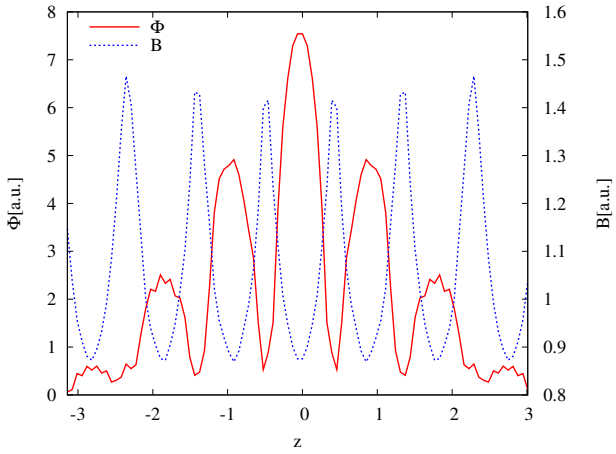

Figure 8. The electrostatic potential ϕ (solid line) along the field line and the magnetic field strength B (dashed line) along the field line, displaying a characteristic trapped-particle mode. Modes of this structure were observed almost everywhere in the parameter space.

In order to gauge the nature of the instabilities observed in our simulations, it is useful to compare the mode frequency ω with the bounce frequency of both the electrons and the ions. For the quasi-isodynamic high-β-case, the most unstable mode observed at high density gradient and with a high $k_y\rho$ had a ratio of $\omega/\omega_{be} \approx (0.22 - 0.27)$, while the majority of modes observed had lower frequencies. The frequencies are thus in general higher than the ion bounce frequency ω_{bi} but below the electron bounce frequency ω_{be},

$$\omega_{bi} < \omega < \omega_{be}.$$

As already mentioned, for instabilities of this kind it can be shown analytically that at the point of marginal stability only modes travelling in the ion direction exist, and they would need to be driven by the ions rather than the electrons. The modes we found in the quasi-isodynamic high-β-configuration indeed had a positive frequency, i.e. they were propagating in the ion diamagnetic direction. Now we pick two modes very close to the point of marginal stability - for the vacuum case $a/L_{T_e} = 1.0$, $a/L_n = 1.5$ and $k_y\rho = 0.8$, for the high-β case the same gradients but $k_y\rho = 0.3$ - and analyse the energy transfer from the particles to the mode with an energy diagnostic built into GENE by A. Bañón Navarro [12]. While for the vacuum case (Fig. 9) both electrons and ions drive the instability, it is only the ions in the high-β-case (Fig. 10) that pump energy into the mode while the electrons - as predicted analytically - draw energy from the instability. It is thus not surprising that the quasi-isodynamic high-β-case is more stable than the vacuum case.

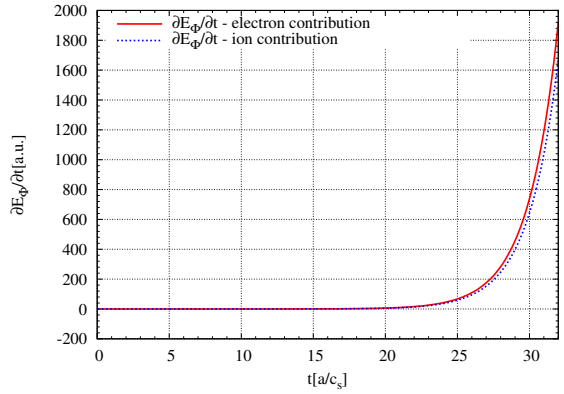

Figure 9. Change of electrostatic energy of the mode due to the electrons (solid line) and the ions (dashed line) in the vacuum configuration.

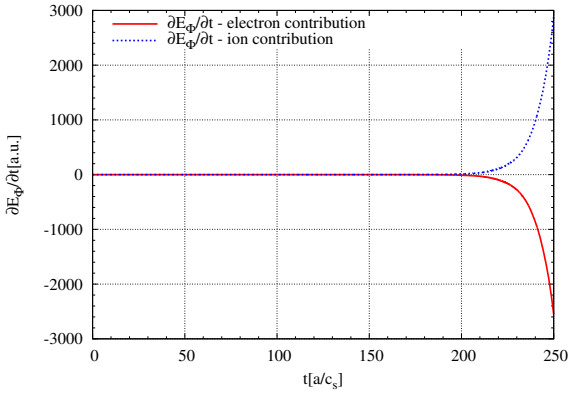

Figure 10. Change of electrostatic energy of the mode due to the electrons (solid line) and the ions (dashed line) in the high-β configuration.

5. Conclusions and Outlook

In this paper we have presented electrostatic trapped-particle mode simulations in an almost perfectly quasi-isodynamic stellarator with $\beta = 6\%$ and the corresponding non-quasi-isodynamic vacuum configuration. Extensive scans over both electron temperature gradient and density gradient revealed a stabilising influence of the temperature gradient for both cases and significantly reduced growth rates for the quasi-isodynamic configuration. While no critical density gradient could be found for the vacuum case, there was a very clear critical gradient at $a/L_n = 0.5$ in the high-β-case, and the growth rates were much smaller. An analysis of the modes found in the high-β-case showed pronounced peaks of the mode structure in the magnetic wells, thus pointing at a trapped-particle mode. In the energy transfer diagnostic it was revealed that for the vacuum case both ions and electrons were driving the mode close to marginal stability while for the quasi-isodynamic configuration only the ions were providing the drive (through their density gradient) whereas the electrons were drawing energy from the mode. This is consistent with the analytical calculations discussed in Sec. 2.

It must be kept in mind that here only one particular flux tube was simulated. Further simulations using other flux tubes are thus required to strengthen the results. Ultimately simulations of an entire flux surface, or the entire plasma volume, might be required. Other configurations should be tested as well, such as Wendelstein 7-X, which is also approaching quasi-isodynamicity, or LHD and NCSX.

Acknowledgments
The authors wish to thank Frank Jenko, Thomas M Bird, Daniel Told, Tobias Görler and Gabriel G Plunk for the fruitful discussions as well as Yuriy Turkin for his help with the visualisation. We would also like to thank Mikhail Mikhailov for providing us with the equilibrium files and Alejandro Bañón Navarro for providing the energy diagnostic. Some of the GENE calculations were performed on the Helios supercomputer (Japan).

References

[1] A A Subbotin, M I Mikhailov, V D Shafranov, M Yu Isaev, J Nührenberg, C Nührenberg, R Zille, V V Nemov, S V Kasilov, V M Kalyuzhnyj and W A Cooper 2006 *Nucl. Fusion* **46** 921
[2] J H E Proll, P Helander, J W Connor and G G Plunk 2012 *Phys Rev. Lett.* **108** 245002
[3] P Helander and J Nührenberg 2009 *Plasma Phys. Control. Fusion* **51** 055004
[4] J Nührenberg 2010 *Plasma Phys. Control. Fusion* **52** 124003
[5] M I Mikhailov, V D Shafranov and J Nührenberg 2009 *Plasma Phys. Rep.* **35** 529
[6] A A Schekochihin, S C Cowley, W Dorland, G W Hammett, G G Howes, E Quaetaert and T Tatsuno 2009 *Ap. J. (Suppl. Series)* **182** 310
[7] F Jenko, W Dorland, M Kotschenreuther and B N Rogers 2000 *Phys. Plasmas* **7** 1904
[8] T Dannert and F Jenko 2005 *Phys. Plasmas* **12** 072309
[9] M J Püschel, M Kammerer and F Jenko 2008 *Phys.Plasmas* **15** 102310
[10] M J Püschel and F Jenko 2012 *Phys. Plasmas* **17** 062307
[11] A M Dimits, G Bateman, M A Beer, B I Cohen, W Dorland, G W Hammett, C Kim, J E Kinsey, M Kothschenreuther, A H Kritz, L L Lao, J Mandrekas, W M Nevins, S E Parker, A J Redd and D E Shumaker 2000 *Phys. Plasmas* **7** 969
[12] A Bañón Navarro, P Morel, M Albrecht-Marc, D Carati, F Merz, T Görler and F Jenko 2011 *Phys. Rev. Lett.* **106** 055001